

# Intensity-Based Axial Localization at the Quantum Limit

J. Řeháček,<sup>1</sup> M. Paúr,<sup>1</sup> B. Stoklasa,<sup>1</sup> D. Koutný,<sup>1</sup> Z. Hradil,<sup>1</sup> and L. L. Sánchez-Soto<sup>2,3</sup>

<sup>1</sup>Department of Optics, Palacký University, 17. listopadu 12, 771 46 Olomouc, Czech Republic

<sup>2</sup>Departamento de Óptica, Facultad de Física, Universidad Complutense, 28040 Madrid, Spain

<sup>3</sup>Max-Planck-Institut für die Physik des Lichts, Staudtstraße 2, 91058 Erlangen, Germany

We derive fundamental precision bounds for single-point axial localization. For the case of a Gaussian beam, this ultimate limit can be achieved with a single intensity scan, provided the camera is placed at one of two optimal transverse detection planes. Hence, for axial localization there is no need of more complicated detection schemes. The theory is verified with an experimental demonstration of axial resolution three orders of magnitude below the classical depth of focus.

**Introduction.**— The maximum spatial resolution attainable in classical microscopy is usually established in terms of the Abbe-Rayleigh criterion [1, 2]. However, it is notorious that this criterion is based on heuristic notions and is an inadequate performance measure for current quantitative imaging [3].

Indeed, several modern techniques, gathered under the broad denomination of superresolution microscopy [4–8], are capable of achieving a striking increase in resolution by more than one order of magnitude in comparison with the length scale set by the Abbe-Rayleigh criterion. An important class of these techniques (which includes, among others, stimulated-emission-depletion microscopy [9], photoactivated-localization microscopy [10], PSF engineering [11–15], and multiplane detection [16–18]) relies on a very accurate localization of point sources.

For three-dimensional imaging, extracting the emitter axial position is an enduring challenge that has been extensively investigated [19]. Yet, finding the optimal depth precision attainable by any such microscope engineering approach has been only recently tackled [20, 21]. The basic idea is to use the quantum Fisher information (qFI) and the associated Cramér-Rao bound (qCRB) to get a measurement-independent limit [22], much in the same vein as Tsang and coworkers did to quantify two-point resolution [23–26].

In this Letter, we address this fundamental question from a different perspective. By identifying the unitary transformation that embodies the action of the system and its corresponding generator, we get in a very transparent way the ensuing qCRB. More important, we do find the optimal measurement reaching such a limit.

We focus here on direct imaging, for this is the simplest method available in the laboratory. Of course, one could rightly argue that in this way all the phase information is wasted. Surprisingly, we demonstrate that direct detection can saturate the quantum limits with a single intensity scan, as long as the camera is placed in one optimal transverse detection plane. This might be of utmost importance for any application demanding extreme stringent localization, as it only requires very simple and feasible equipment.

**Theoretical model.**— To simplify the details as much as possible, we take the waist of a focused beam as our object. The task is to estimate the distance from this object to a detection plane. In the following, we use the Dirac notation to represent the field, as it allows to extend the theory to any type of light source.

If the beam in the object plane is represented by the pure state  $|\Psi(0)\rangle$ , the axial displacement is described by a unitary operation

$$|\Psi(z)\rangle = e^{iGz} |\Psi(0)\rangle, \quad (1)$$

the Hermitian operator  $G$  being corresponding generator. To identify the action of  $G$  in a more precise way, it is convenient to use the transverse-position representation  $\Psi(x, y; z) = \langle x, y | \Psi(z) \rangle$ . Given the form of Eq. (1), we have that

$$\partial_z \Psi(x, y; z) = iG \Psi(x, y; z), \quad (2)$$

which is consistent with the paraxial wave equation  $2ik\partial_z \Psi(x, y; z) = \nabla_T^2 \Psi(x, y; z)$  if

$$G \mapsto \frac{1}{2k} \nabla_T^2, \quad (3)$$

where  $k$  is the wavenumber and  $\nabla_T^2 = \partial_{xx} + \partial_{yy}$  is the transverse Laplacian.

For a more tractable analysis and experiment, here we assume a normalized Gaussian beam

$$\Psi(r; z) = \frac{2}{w(z)} e^{-\frac{r^2}{w^2(z)}} \exp\left(-i\left[kz + \frac{kr^2}{2R(z)} - \phi(z)\right]\right), \quad (4)$$

although the results are largely independent of this choice. Notice that, given the cylindrical symmetry, the beam depends exclusively on the radial coordinate  $r$ . The field distribution in Eq. (4) is determined by the beam waist  $w_0$  and the Rayleigh range  $z_R$  through  $w^2(z) = w_0^2[1 + (z/z_R)^2]$ ,  $R(z) = z[1 + (z_R/z)^2]$ ,  $\phi(z) = \arctan(z/z_R)$ , and  $z_R = \pi w_0^2/\lambda$ .

The detection plane is placed at  $z$  and therein we perform a measurement that we do not need to specify by the time being. To quantify the information about  $z$  available in the measured signal we use the qFI, which, for pure states, as it is our case, is given by  $\mathcal{Q}(z) = 4 \text{Var}(G)$ , where  $\text{Var}$  is the variance computed in the initial state. Given the representation (3) for  $G$ , a direct calculation shows that for the Gaussian beam one has

$$\mathcal{Q}(z) = \frac{1}{z_R^2}, \quad (5)$$

which turns out to be constant. The qCRB [27, 28] ensures then that the variance of any unbiased estimator  $\hat{z}$  of the displacement  $z$  is bounded by the reciprocal of the qFI;

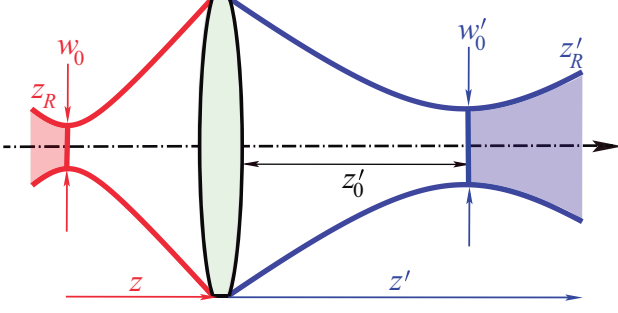


FIG. 1. Scheme of the axial localization experiment with a relay optical system.

viz,  $\text{Var}(\hat{z}) \geq 1/\mathcal{Q}(z)$ . In consequence, the lower bound on axial-measurement errors (per single detection) is precisely the Rayleigh range. This agrees with the result recently found in Ref. [29], which discusses the ultimate limits for two-point axial resolution.

*Direct detection.*— In general, the qFI would be distributed between the phase and intensity variations of the measured beam. One would naively expect that intensity detection, discarding all phase information, cannot saturate the quantum limit (5). We will show that, contrary to this belief, this is not the case when the detector is appropriately placed.

We model the light detection as a random process and, consequently, we interpret the normalized beam intensity  $p(r|z) = |\Psi(r; z)|^2$  as the probability density of a single detection event at  $r$  conditional on the value of  $z$ . We assume that detection is limited by shot noise, which obeys a Poisson distribution [30]. This simplified approach ignores nonclassical effects, as bunching or entanglement, but is nonetheless relevant to practical microscopy. In addition, we ignore finite spatial extent and nonzero pixel size. Under these hypothesis, the classical Fisher information about  $z$  per single detection is

$$\mathcal{F}(z) = 2\pi \int_0^\infty r \frac{[\partial_z p(r|z)]^2}{p(r|z)} dr, \quad (6)$$

and the associated CRB quantifies the axial localization error for direct detection. For a Gaussian beam,  $p(r|z) = [\pi w^2(z)/2]^{-1} \exp[-2r^2/w^2(z)]$ , so that

$$\mathcal{F}(z) = \frac{\partial_z w^2(z)}{w^2(z)} = \frac{1}{4R^2(z)} = \frac{1}{4z[1 + (z_R/z)^2]}. \quad (7)$$

Optimal detector positions are at the planes of maximal wavefront curvature:  $z_{\text{opt}} = \pm z_R$ , whereby the quantum limit is saturated; i.e.,  $\mathcal{F}_{\text{opt}} = \mathcal{Q}$ . In these planes, all the information about the axial waist location is encoded in the intensity and can be extracted with conventional imaging, thus avoiding more complicated and less robust techniques.

Potential applications of this effect benefit from using a relay optical system for reimagining the object and obtaining a more convenient detector position. Figure 1 sketches the simplest case of a thin lens placed a distance  $z$  from the waist.

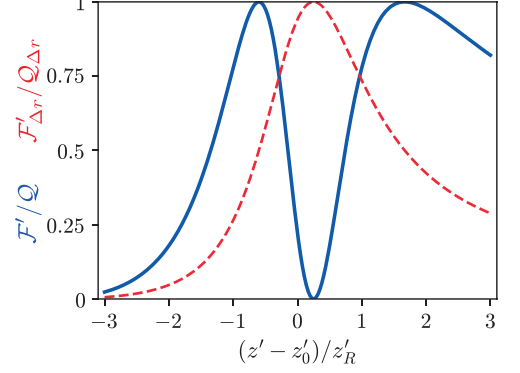


FIG. 2. Fisher information in the image space in units of quantum Fisher information for different positions of the detector. We use  $z = 5$ ,  $f = 1$ ,  $z_R = 1$ ,  $w_0 = 1$  and the detector positions are relative to the beam waist in units of  $z'_R$ .

Primed symbols will distinguish henceforth parameters in the image space.

Since the ideal imaging system applies a unitary transformation, the qFI does not change from the object space to the image space:  $\mathcal{Q}' = \mathcal{Q}$ . Recalling the standard relations [31]

$$w_0'^2 = m^2 w_0^2, \quad z'_R = m^2 z_R, \quad z'_0 = m^2(z - f) + f, \quad (8)$$

between the original and new beam parameters, where  $m^2 = f^2/[(z - f)^2 + z_R^2]$  is the magnification, we find the beam width at the detector position  $z'$  to be

$$w'^2(z') = w_0'^2 \left[ 1 + \left( \frac{z' - z'_0}{z'_R} \right)^2 \right]. \quad (9)$$

Much in the same way as in Eq. (7), we have now

$$\begin{aligned} \mathcal{F}'(z) &= \frac{\partial_{z'} w'^2(z')}{w'^2(z')} \\ &= \frac{4(f - z')^2 [zz' - f(z + z')]^2}{(z^2 + z_R^2)z'^2 - 2fz'(z^2 + z_R^2 + zz') + f^2[(z + z')^2 + z_R^2]}. \end{aligned} \quad (10)$$

The typical behavior of  $\mathcal{F}'$  around the beam waist is shown in Fig. 2. We observe the presence of well-resolved maxima and minima. While the beam in the image space is symmetric about the waist, the response of the beam width to small changes of the true distance  $z$  is different inside and outside the waist, which makes the FI asymmetrical with respect to the image waist. These extremal points are located at

$$z'_{\text{opt}} = \begin{cases} z'_0 + \alpha z'_R, \\ z'_0 - \frac{1}{\alpha} z'_R, \end{cases} \quad (11)$$

where  $\alpha = (f - z - z_R)/(f - z + z_R)$ . In the geometrical limit  $f - z \gg z_R$ , we have  $\alpha \simeq 1$  and  $z'_{\text{opt}} \approx z'_0 \pm z'_R$ , so the asymmetry disappears. Interestingly, information about axial

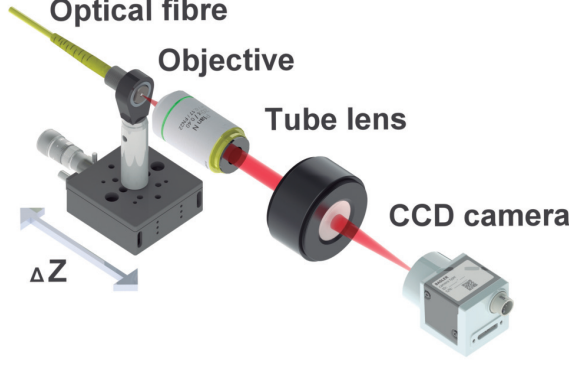


FIG. 3. Experimental setup used to measure the axial displacement  $z$ . See text for a detailed description.

displacements is zero in the plane of the geometrical image  $z' = fz/(z-f)$ , as the FI tends to zero therein. In this sense, optimal axial localization (requiring considerable image blur) and transverse localization (benefiting from sharpness) complement each other. PSF engineering reaches a balance to resolve this issue and provides a good three-dimensional resolution. However, these methods always broaden the PSF, even more than our defocusing in  $z_R$ .

*Experiment.*— To check the previous theory we have used a classical microscopy setup, as schematized in Fig. 3. It consists of an objective corrected for infinity and a tube lens, all together providing a  $20\times$  magnification of the output face of a single mode fiber representing a Gaussian source. The fiber is coupled with a 632.8 nm He-Ne laser. As the Rayleigh range  $z_R$  at the fiber output is  $18.9\ \mu\text{m}$ , the camera with  $5.5\ \mu\text{m}$  is moved 7.6 mm out of the system nominal image plane to become aligned with one of the optimal detection positions given in Eq. (11). Controlled changes of the axial distance  $z$  were implemented by moving the fiber axially using a piezo stage with a resolution of 1 nm.

Note that the integrand in Eq. (6); viz,

$$F(r; z) = r \frac{[\partial_z p(r|z)]^2}{p(r|z)} \quad (12)$$

can be seen as a radial density of Fisher information. This magnitude is plot in Fig. 4 at the optimal detection plane, which hints at constructing a robust estimator of axial displacement from the registered intensity scans. The information drops to zero at  $r_b = w'_0/\sqrt{2}$  and the bulk of information ( $2/e \simeq 74\%$ ) resides outside this boundary in the wings of the Gaussian intensity distribution. We will call  $I_{\text{det}}(z)$  the intensity outside  $r_b$  for the object distance  $z$ . Then for small displacements  $\delta_z$  from the nominal position  $z$  we have

$$I_{\text{det}}(z + \delta_z) = I_{\text{det}}(z)(1 - \delta_z/z_R). \quad (13)$$

This linear relation is readily inverted to yield an estimate  $\hat{\delta}_z$  of  $\delta_z$  from  $I_{\text{det}}$ . Of course, we might be tempted to use

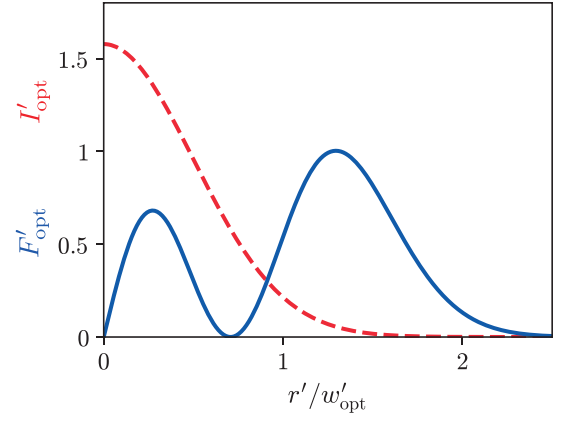


FIG. 4. Normalized radial density of Fisher information (solid blue line) and normalized beam intensity profile (dashed orange line) in the optimal detection plane, where the beam has a width  $w'_{\text{opt}}$ . The system parameters are the same as in Fig. 2.

the maximum likelihood estimator based on the full profile. However, this estimator turns to be a bit noisy due to systematic errors [32]. On the contrary, our estimator  $\hat{\delta}_z$  is simple and robust. Nevertheless, we stress that we are interested in a proof-of-concept experiment, so small deviations from the theoretical best performance are non issue.

We also notice that we are assuming that the nominal axial distance is known. This is not a serious drawback, as one can perform a previous calibration (as we did in the experiment), and then measure in a very precise manner around the nominal value.

Our experimental results are summarized in Fig. 5. Measurement errors are consistent across the full range of axial displacements  $\delta_z \in [10\ \text{nm}, 1650\ \text{nm}]$  averaging 24.8 nm. This is about 800 times below the depth of focus  $z_R$  and not much above the quantum limit of 14.9 nm corresponding to the total number of  $1.6 \times 10^6$  detections registered for each  $\delta_z$  setting.

Thus far we have focused on axial measurements with Gaussian beams. What about *uncooperative* point sources? In this case, the source generates a spherical (paraboidal) wavefront, which after transiting a distance  $z$  enters an imaging system that truncates the unbounded wave with a pupil function. Keeping things simple and considering a Gaussian pupil transmissivity of width  $w_l$  the wave on the pupil depends on  $z$  through

$$U(x, y; z) = \sqrt{\frac{2}{\pi w_l^2}} \exp \left[ -\frac{r^2}{w_l^2} - i \frac{kr^2}{2(z-f)} \right]. \quad (14)$$

The state in the aperture is not just axial propagation from the point source, as the pupil acts like a filter and one needs to renormalize the state. The process is now not unitary and the qFI cannot be calculated in terms of a generator  $G$ . Instead, one has

$$\frac{1}{4} \mathcal{Q}(z) = \langle \partial_z \Psi(z) | \partial_z \Psi(z) \rangle - \langle \partial_z \Psi(z) | \Psi(z) \rangle \langle \Psi(z) | \partial_z \Psi(z) \rangle. \quad (15)$$

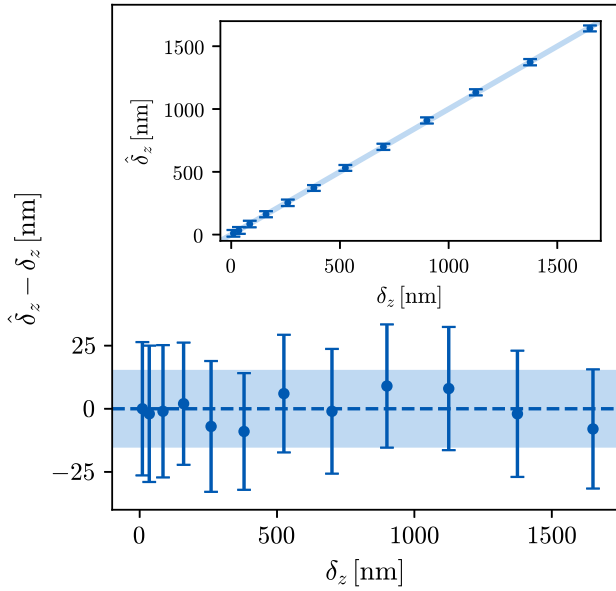


FIG. 5. Experimental estimation of axial displacements  $\delta_z$  from the nominal object plane with respect to which the camera is optimally placed (11). The inset shows the statistics of the estimator  $\hat{\delta}_z$  as defined in Eq. (13). In the main plot the true distance was subtracted from the estimates to get a more convenient scale on the vertical axis. The blue strips depict the quantum bound for the  $2 \times 10^6$  detections and  $z_R = 18.9 \mu\text{m}$ .

At difference of a Gaussian source, the result now reads

$$\mathcal{Q}(z) = \frac{k^2 w_l^4}{4z^4}, \quad (16)$$

which strongly depends on the true distance  $z$ . We mention in passing that, like for a Gaussian source, this qFI can be saturated with a single intensity scan optimally placed with respect to the nominal image plane. It is intriguing to note that  $n = 2 \times 10^6$  detections like in our experiment registered with a one meter aperture  $w_l = 1 \text{ m}$  in visible light  $k = 10^7 \text{ m}^{-1}$  would theoretically provide axial localization of a point source in a low Earth orbit  $z = 200 \text{ km}$  with about 5 m accuracy.

In conclusion, we have theoretically and experimentally demonstrated the axial superresolution based on direct detection. The quantum limits can be saturated with a single intensity scan provided the camera is placed in one of two optimal transversal detection planes. Hence for axial localization problem there is no advantage in adopting more complicated detection schemes. Our method makes three-dimensional superresolution imaging promising and can be potentially useful for enhancing the resolution of optical microscopes.

We thank Robert W. Boyd for helpful discussions. We acknowledge financial support from the Grant Agency of the Czech Republic (Grant No. 18-04291S), the Palacký University (Grant No. IGA\_PrF\_2019-007), and the Spanish MINECO (Grant FIS2015-67963-P).

- 
- [1] Lord Rayleigh, “Investigations in Optics, with special reference to the spectroscope,” *Phil. Mag.* **8**, 261–274, 403–411, 477–486 (1879).
  - [2] E. Abbe, “Ueber einen neuen Beleuchtungsapparat am Mikroskop,” *Arch. Mikrosk. Anat.* **9**, 469–480 (1873).
  - [3] S. Ram, E. S. Ward, and R. J. Ober, “Beyond Rayleigh’s criterion: A resolution measure with application to single-molecule microscopy,” *PNAS* **103**, 4457–4462 (2006).
  - [4] S. W. Hell, “Far-field optical nanoscopy,” *Science* **316**, 1153–1158 (2007).
  - [5] B. Huang, M. Bates, and X. Zhuang, “Super-resolution fluorescence microscopy,” *Annu. Rev. Biochem.* **78**, 993–1016 (2009).
  - [6] G. Huszka and M. A. M. Gijs, “Super-resolution optical imaging: A comparison,” *MNE* **2**, 7–28 (2019).
  - [7] L. Schermelleh, R. Heintzmann, and H. Leonhardt, “A guide to super-resolution fluorescence microscopy,” *J. Cell Biol.* **190**, 165 (2010).
  - [8] B. O. Leung and K. C. Chou, “Review of super-resolution fluorescence microscopy for biology,” *Appl. Spectrosc.* **65**, 967–980 (2011).
  - [9] S. W. Hell and J. Wichmann, “Breaking the diffraction resolution limit by stimulated emission: stimulated-emission-depletion fluorescence microscopy,” *Opt. Lett.* **19**, 780–782 (1994).
  - [10] E. Betzig, G. H. Patterson, R. Sougrat, O. W. Lindwasser, S. Olenych, J. S. Bonifacino, M. W. Davidson, J. Lippincott-Schwartz, and H. F. Hess, “Imaging intracellular fluorescent proteins at nanometer resolution,” *Science* **313**, 1642 (2006).
  - [11] B. Huang, W. Wang, M. Bates, and X. Zhuang, “Three-dimensional super-resolution imaging by stochastic optical reconstruction microscopy,” *Science* **319**, 810 (2008).
  - [12] S. R. P. Pavani, M. A. Thompson, J. S. Biteen, S. J. Lord, N. Liu, R. J. Twieg, R. Piestun, and W. E. Moerner, “Three-dimensional, single-molecule fluorescence imaging beyond the diffraction limit by using a double-helix point spread function,” *Proc. Natl. Acad. Sci. USA* **106**, 2995 (2009).
  - [13] S. Jia, J. C. Vaughan, and X. Zhuang, “Isotropic three-dimensional super-resolution imaging with a self-bending point spread function,” *Nat. Photonics* **8**, 302 (2014).
  - [14] F. Tamburini, G. Anzolin, G. Umbriaco, A. Bianchini, and C. Barbieri, “Overcoming the Rayleigh criterion limit with optical vortices,” *Phys. Rev. Lett.* **97**, 163903 (2006).
  - [15] M. Pař, B. Stoklasa, J. Grover, A. Krzic, L. L. Sánchez-Soto, Z. Hradil, and J. Řeháček, “Tempering Rayleigh’s curse with PSF shaping,” *Optica*, *Optica* **5**, 1177–1180 (2018).
  - [16] P. A. Dalgarno, H. I. C. Dalgarno, A. Putoud, R. Lambert, L. Paterson, D. C. Logan, D. P. Towers, R. J. Warburton, and A. H. Greenaway, “Multiplane imaging and three dimensional nanoscale particle tracking in biological microscopy,” *Opt. Express* **18**, 877–884 (2010).
  - [17] M. F. Juette, T. J. Gould, M. D. Lessard, M. J. Mlodzianoski, B. S. Nagpure, B. T. Bennett, S. T. Hess, and J. Bewersdorf, “Three-dimensional sub-100 nm resolution fluorescence microscopy of thick samples,” *Nat. Methods* **5**, 527 (2008).
  - [18] S. Abrahamsson, J. Chen, B. Hajj, S. Stallinga, A. Y. Katsov, J. Wisniewski, G. Mizuguchi, P. Soule, F. Mueller, C. D. Darzacq, X. Darzacq, C. Wu, C. I. Bargmann, D. A. Agard, M. Dahan, and M. G. L. Gustafsson, “Fast multicolor 3D imag-

- ing using aberration-corrected multifocus microscopy,” *Nat. Methods* **10**, 60 (2012).
- [19] A. von Diezmann, Y. Shechtman, and W. E. Moerner, “Three-dimensional localization of single molecules for super-resolution imaging and single-particle tracking,” *Chem. Rev.* **117**, 7244–7275 (2017).
- [20] M. Tsang, “Quantum limits to optical point-source localization,” *Optica* **2**, 646–653 (2015).
- [21] M. P. Backlund, Y. Shechtman, and R. L. Walsworth, “Fundamental precision bounds for three-dimensional optical localization microscopy with Poisson statistics,” *Phys. Rev. Lett.* **121**, 023904 (2018).
- [22] D. Petz and C. Ghinea, “Introduction to Quantum Fisher Information,” in *Quantum Probability and Related Topics*, Vol. Volume 27 (World Scientific, 2011) pp. 261–281.
- [23] M. Tsang, R. Nair, and X.-M. Lu, “Quantum theory of super-resolution for two incoherent optical point sources,” *Phys. Rev. X* **6**, 031033 (2016).
- [24] R. Nair and M. Tsang, “Far-field superresolution of thermal electromagnetic sources at the quantum limit,” *Phys. Rev. Lett.* **117**, 190801 (2016).
- [25] S. Z. Ang, R. Nair, and M. Tsang, “Quantum limit for two-dimensional resolution of two incoherent optical point sources,” *Phys. Rev. A* **95**, 063847 (2016).
- [26] M. Tsang, “Subdiffraction incoherent optical imaging via spatial-mode demultiplexing,” *New J. Phys.* **19**, 023054 (2017).
- [27] C. W. Helstrom, *Quantum Detection and Estimation Theory* (Academic, New York, 1976).
- [28] A. S. Holevo, *Probabilistic and Statistical Aspects of Quantum Theory*, 2nd ed. (North Holland, Amsterdam, 2003).
- [29] Y. Zhou, J. Yang, J. D. Hassett, S. M. H. Rafsanjani, M. Mirhosseini, A. N. Vamivakas, A. N. Jordan, Z. Shi, and R. W. Boyd, “Quantum-limited estimation of the axial separation of two incoherent point sources,” *Optica* **6**, 534–541 (2019).
- [30] D. R. Fuhrmann, C. Preza, J. A. O’Sullivan, D. L. Snyder, and W. H. Smith, “Spectrum estimation from quantum-limited interferograms,” *IEEE Trans. Signal Process.* **52**, 950–961 (2004).
- [31] A.E. Siegman, *Lasers* (Oxford University Press, Oxford, 1986).
- [32] C. S. Smith, N. Joseph, B. Rieger, and K. A. Lidke, “Fast, single-molecule localization that achieves theoretically minimum uncertainty,” *Nat. Methods* **7**, 373 (2010).